LAWRENCE
LIVERMORE
NATIONAL
LABORATORY

LLNL-JRNL-817509

Spectroscopic Signatures of MQ-Resins in Silicone Elastomers

A. Sawvel, J. Crowhurst, H. Mason, J. Oakdale, S. Ruelas, H. Eshelman, R. Maxwell

December 9, 2020

Macromolecules

Disclaimer

Spectroscopic Signatures of MQ-Resins in Silicone Elastomers

April M. Sawvel[1], Jonathan C. Crowhurst[1], Harris E. Mason[2], James S. Oakdale[1], Samantha Ruelas[1], Hannah V. Eshelman[1], and Robert S. Maxwell[,1].*

[1]Physical and Life Sciences Directorate, Materials Science Division, Lawrence Livermore National Laboratory, 7000 East Avenue, Livermore, CA 94550.

[2]Physical and Life Sciences Directorate, Atmospheric, Earth, and Energy Division, Lawrence Livermore National Laboratory, 7000 East Avenue, Livermore, CA 94550.

For Table of Contents Use Only (TOC Graphic):

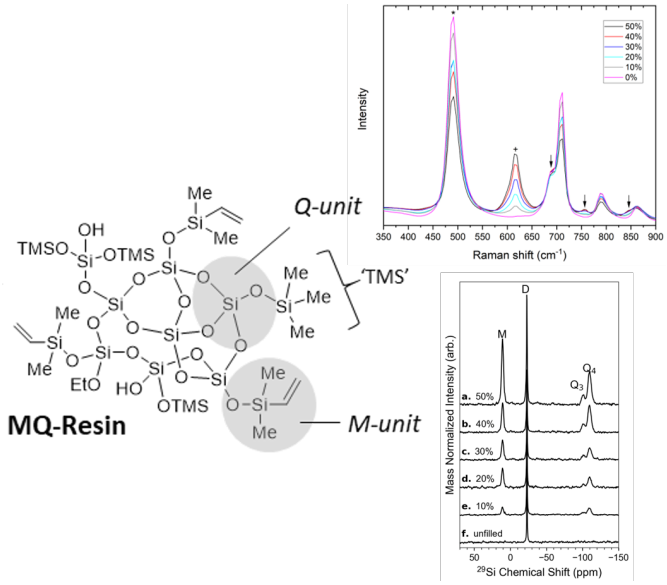

LLNL-JRNL-817509

ABSTRACT: Polysiloxane elastomers have a large application space due to their versatile cross-linking chemistry and highly tunable physical and mechanical properties. One approach for improving the mechanical integrity of commercial polysiloxane 'silicone' elastomers while maintaining their optical transparency is the addition of small, silicone-resin molecules to the network. However, both the PDMS network and the silicone-resin particles have an amorphous structure and complex chemistry which makes the characterization of their structural properties and segmental network dynamics difficult. Here, we report the synthesis and characterization of a series of model silicone networks modified with a specific class of silicone-resin known as MQ-resin using Raman and advanced nuclear magnetic resonance (NMR) spectroscopy methods. Raman spectroscopy was successfully used to quantify the contribution of the MQ-resin to the network, to determine the type of MQ-resin present in the network, and to investigate completeness of the network cross-linking reaction. Solid-state and ^{1}H double-quantum (DQ) NMR spectroscopies were used not only as a detection method for the MQ-resins, but also to quantify changes in the segmental dynamics of the network as a function of MQ-resin concentration. The combination of Raman and NMR spectroscopies describe a series of samples where the MQ-resin particles and PDMS chains maintain their independent segmental dynamics up to high concentrations of MQ-resin (40-50% MQ), where the physical properties of the resin dominate the physical properties of the overall network. The results from our spectroscopic analyses are consistent with the results from macroscopic characterization techniques such as solvent uptake and mechanical testing. The spectroscopic insights into the structure-property relationships of PDMS-MQ composites presented in this study are a valuable tool not only for the synthesis and reverse engineering of future generations of commercial silicone elastomers, but also for understanding the mechanisms of aging and degradation over the material lifetime.

LLNL-JRNL-817509

INTRODUCTION

Polysiloxane elastomers, otherwise known as silicone rubbers, make up an important class of semi-inorganic polymers valued for their unique combination of desirable properties, including exceptional thermal stability, chemical inertness, low off-gassing, high gas permeability, and a unique ability to maintain useful properties over a wide range of service temperatures (> -100 ºC to >250 ºC).[1, 2] As such, these materials find use in a wide variety of applications ranging from everyday consumer items (e.g. utensils, baby feeding bottles), medical devices (e.g. prosthetics or catheters), and as general sealants (i.e. gaskets and caulking) to meet the diverse needs of automotive, aerospace and construction sectors. All high-performance 'silicones' of commercial interest can be classified as composites consisting of crosslinked polysiloxane networks reinforced with particulate filler.[3] In most instances, fillers are added with the primary purpose of improving mechanical properties and filler materials commonly utilized within silicone rubbers include finely divided silicas, carbon black, or diatomaceous earth.

An additional subset of polysiloxanes are the so-called siloxane- or silicone-resins, which are highly-branched macromolecules composed of one or more primary silicone structural units - M ($R_3SiO_{1/2}$), D ($R_2SiO_{2/2}$), T ($RSiO_{3/2}$) and/or Q ($SiO_{4/2}$) (Scheme 1).[4] These materials are used in a broad range of applications, notably as damping agents in pressure sensitive adhesives,[5-7] glossing or tackifying agents in cosmetic formulations, [8]and notably, as reinforcing agents in siloxane elastomers.[9, 10] While many different types of silicone-resins exist (MQ, MT, TD, T, MTQ, etc.), we have focused our efforts specifically on characterizing vinyl functionalized MQ-resins (named for their repeating "M" and Q" structural units, Scheme 1a) incorporated into polydimethylsiloxane (PDMS) elastomers. MQ-resins are commercially available but can also be easily prepared through a several methods, including a simple one-pot two-step process shown in

Scheme 1a.[11, 12] Here, alkyl silicates (Q-unit precursor) are co-hydrolyzed in presence of reactive trialkylsilyl compounds (M-unit precursor) to arrive at an MQ species containing a silicate core ($SiO_{4/2}$) decorated with trimethylsilyl and dimethyl(vinyl)silyl functional groups. The MQ copolymers that result from these sol-gel reactions are polydisperse and the MQ-resin presented in scheme 1a is only one of many hypothetical structures.[11] Likewise, Scheme 1b illustrates the formation of a MQ-resin reinforced hypothetical silicone elastomer resulting from the addition of vinyl-terminated PDMS and vinylated MQ-resin to methylhydrosiloxane crosslinkers.

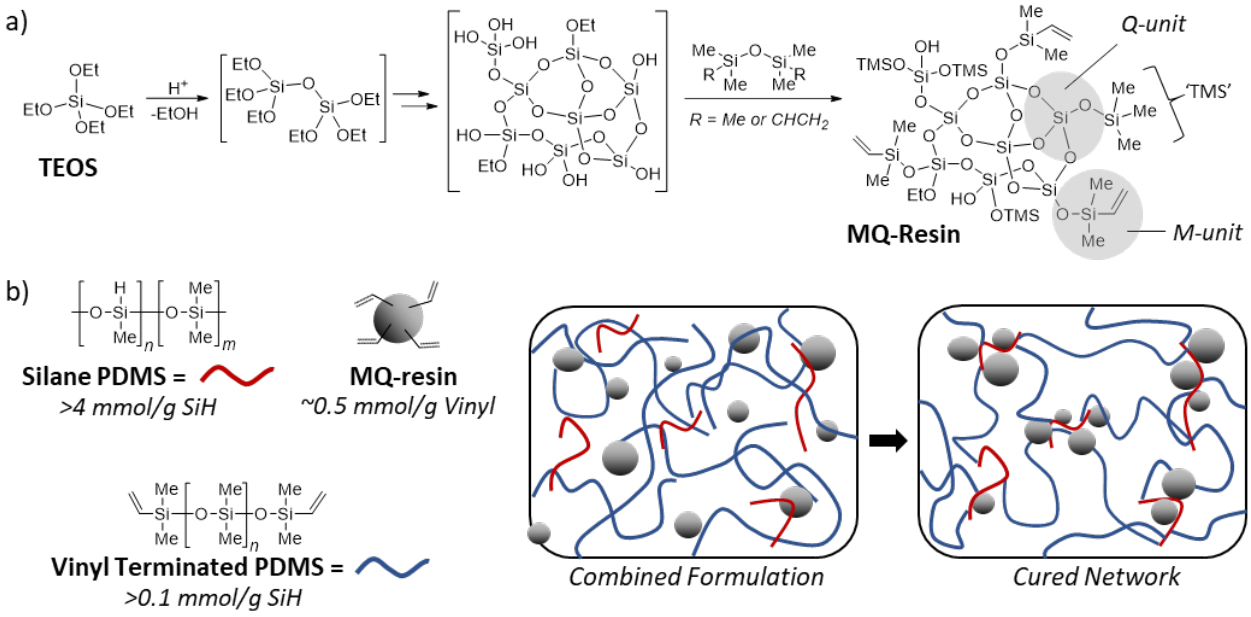

Scheme 1. a) Hydrolysis of alkyl-silicates to form a theoretical MQ resin structure. b) Hypothetical siloxane network resulting of vinylated MQ resin cross-linked with PDMS chains via platinum catalyzed hydrosilylation.

MQ species have multiple chemical junction points in the silicone network, both covalent bonding via vinyl functionality in addition to potential non-covalent interactions such as Van der

Waals, electrostatic, or hydrogen bonding with the polymer backbone or side groups that are dependent on the amount, surface chemistry and size of the MQ-resin. The result is a structurally complex composite with a broad range of polymer and particle dynamics. The MQ-resins are typically added during formulation but can also form during the curing process. For example, polysiloxane mixing conditions such as the presence of excess crosslinker, moisture, and the implementation of an elevated-temperature post-curing step can lead to unwanted condensation reactions that produce silicone-resins within the network. As a result, many silicone networks can have unintended silicone-resin species present that can lead to non-ideal behavior.[13-15]

Ultimately, the dynamics of polymer-filler interactions and their influence on mechanical and thermal properties is of utmost importance for understanding and predicting the lifetime and aging of silicone components. Given the strong influence these species can have on silicone composites, improved methods to detect and quantify MQ species and improved insight into how MQ species influence polymer segmental dynamics and mechanical properties are needed. There are few spectroscopic methods that specifically identify MQ and/or quantify its concentration in commercial silicones or model networks. Both Raman spectroscopy and solid-state nuclear magnetic resonance (NMR) methods provide routes to achieve the detection and quantification of MQ species.

Raman spectroscopy is an obvious candidate for detecting MQ species and chemistry given the strength of the Raman scattering process in both the MQ-resin and the PDMS polymer chain. In addition, the technique is non-destructive, rapid, spatially selective, and requires no special sample handling or treatment. There are many examples in the literature, spanning several decades, of the application of Raman spectroscopy to the study of PDMS and related materials. Some examples include the investigation of strain and temperature on molecular

isomerism by measurements of depolarization,[16] the effect of confinement and shear-induced changes in PDMS thin films,[17] as a tool for the characterization of PDMS-based optical waveguide materials,[18] and the determination of the interaction of zinc oxide nanoparticles with a PDMS polymer matrix.[19] Here, we use Raman spectroscopy to develop a calibration curve for the concentration of MQ-resin in a PDMS network, to determine the M/Q ratio of the MQ-resins studied here, and to monitor the completeness of cross-linking in our networked samples.

Solid-state NMR spectroscopy provides complimentary, elementally specific information about the local bonding environment as well as the local and segmental dynamics over a broad range of timescales in elastomeric samples.[20] Cross-polarization magic angle spinning (CP/MAS) methods, for example, are well known to provide insight into speciation but are sensitive to mobility differences through motional perturbations to the heteronuclear dipolar couplings that govern the CP efficiency. In a highly mobile polymer such as silicone elastomers, the ^{1}H-^{29}Si dipolar couplings are significantly quenched by both the rapid CH_3 rotation around the C3 axis but also the significant segmental dynamics of the chains. A sequence based on the generation of signal through repetitive CP contact times (so called Multi-CP) has shown to ameliorate some of these motional effects and has shown promise in enhancing the $^{13}C\{^{1}H\}$ CP/MAS signal for partially mobile polyolefins.[21] In addition, much effort has been recently devoted to the use of static ^{1}H NMR methods, and Double-Quantum NMR (DQNMR) methods in particular, to quantify the segmental dynamics of silicone networks as a function of formulation, filler content, and aging as well as to gain insight into structure-property relationships in this ubiquitous family of elastomers.[15, 22-32]

Herein, we integrate Raman and NMR spectroscopies to interrogate polysiloxane elastomers reinforced with a particular class of silicone-resins known as MQ-resins. Our

approach advances the ability to assess the impact of the MQ species on the structure and properties of silicone composites and will improve our understanding of the mechanisms and kinetics of "accidental" MQ formation, their effects on structure-property relationships, and any role they may have in aging and degradation mechanisms. The chemical and physical characterization of a series of MQ-resins combined with spectroscopic analyses are used to link the local structure and dynamics of these polymer formulations to their mechanical properties and to reveal the influence of MQ filler on their performance.

EXPERIMENTAL SECTION

Synthesis of MQ-Resin and formulation of MQ silicone elastomers. Vinylated MQ-resins were prepared following a protocol described by Flagg and McCarthy.[11] A 2-neck 500 mL round bottom flask equipped with a stirring bar, reflux condenser and glass stop-cock was charged with 75 mL ethanol and 60 ml water containing 30 µl concentrated sulfuric acid. The reaction vessel was then placed in a 50 °C oil bath and allowed to warm for 10 min. Tetraethyl orthosilicate (60 g, 0.288 mmol) was then added and the reaction was allowed to progress for a 1 h. A mixture of hexamethyldisiloxane (21.87 g, 0.134 mol) and 1,3-divinyltetramethyl disiloxane (2.87 g, 0.015 mol) dissolved in 90 ml toluene was then added, followed shortly thereafter by 3 mL concentrated sulfuric acid. The reaction was warmed to 70 °C and allowed to progress for an additional 3 hours before being removed from the oil bath and cooled to room temperature. The resulting mixture was transferred to a separatory funnel and the lower, organic layer was collected, washed with saturated sodium bicarbonate, and dried over sodium sulfate. The organic extract was finally concentrated via rotary evaporation and dried under high vacuum to yield approximately 40 g of a colorless crystalline solid. The M-to-Q ratio of the resulting product varied from 0.5 to 0.8 depending on the batch and was calculated from ^{1}H spectra as described

by Xu et al.[33] Silicone elastomers containing 0-50 wt% MQ-resin were formulated by first dissolving the MQ-resin fraction in a minimal amount of dichloromethane followed by the addition of vinyl terminated polydimethylsiloxane (DMS-V33 from Gelest). Dichloromethane was then gently removed by subjecting the resinous mixture to a stream of compressed air over a period of 12-24 h. Finally, methylhydrogen siloxane dimethylsiloxane (HMS-H271 Gelest) copolymer was added to the mixture to arrive at a 1.4:1 stoichiometric molar ratio to silane:vinyl. 10 ppm platinum catalyst (SIP6832.2, Gelest) and 30 ppm platinum inhibitor, 2-methylbut-3-yn-2-ol, were added and the formulation was mixed on a FlackTek speed-mixer for 30 s and degassed under vacuum before being cast in sheets or buttons. The material was then cured at 80 °C for period of 6 h, followed by an overnight 150 °C post-cure.

Equilibrium Solvent Uptake Experiments. Solvent swelling measurements were conducted as described elsewhere[15] to determine the percent soluble fraction of material extracted from the network ($\%\omega_{sol}$) and the equilibrium degree of swelling (Q). Three sections of each sample were used to determine an average and standard deviation for each parameter. The $\%\omega_{sol}$ and Q values were calculated using equations 1 and 2.

$$\%\omega_{sol} = \frac{m_i - m_f}{m_i} * 100\% \quad (1)$$

The equilibrium degree of swelling was calculated using the density of PDMS (ρ_{PDMS} = 0.965 g/cm^3) as well as the density of toluene (ρ_{tol} = 0.867 g/cm^3).

$$Q = \frac{V_{sw}}{V_{dry}} = \frac{m_f/\rho_{PDMS} + (m_{sw} - m_i)/\rho_{tol}}{m_f/\rho_{PDMS}} \quad (2)$$

Mechanical Measurements. Tensile testing was performed with ASTM D-638 Type V dumbbell specimen (width 3.18 mm, length 9.53 mm) punched from 2 mm thick sheets at 21-23 °C using an Instron Universal Testing Machine 5944 equipped with pneumatic grips, a 100N load cell and at a crosshead speed rate of 10 mm/min. Strain was recorded as the displacement between the crossheads, Young's modulus was calculated from the resulting stress-strain curve over 0-2%.

Raman Spectroscopy. Raman scattering was excited with a HeNe laser at a wavelength of 632.8 nm. Laser light (~ 20 mW) was focused onto the sample using a Mitutoyo apochromatic 20x objective with a numerical aperture of 0.4. Scattered light was collected through the same objective. A set of filters (OptiGrate) were used to reject the laser line. A pinhole in a confocal arrangement was used to further reject extraneous light and increase spatial resolution. Other than where noted the polarization state of the collected light was not analyzed. Spectra were obtained with a grating spectrometer (PI Acton SP2300) and a cooled CCD detector (Pixis400). Most spectra shown here were obtained with a 300 lines/mm grating. Higher resolution spectra were obtained with an 1800 lines/mm grating. A broadband standard light source was used to correct for the instrumental sensitivity over the wide spectral range provided by the 300 lines/mm grating. Electronic artifacts were removed where necessary. The system was calibrated using a neon standard lamp.

NMR Spectroscopy. The $^{29}Si\{^{1}H\}$ cross polarization (CP) and single pulse (SP) MAS experiments were conducted on a Bruker Avance III spectrometer operating at Larmour frequencies of 399.82 and 79.43 MHz for ^{1}H and ^{29}Si, respectively, using a Bruker HXY MAS probe with 4 mm (o.d.) rotors spinning at 13 kHz. The ^{29}Si SP/MAS data were collected using high power ^{1}H decoupling (r.f. = 130 kHz), a 30° excitation pulse of 1.5 μs (r.f. = 56 kHz) and a

120 s acquisition delay for 1,503 acquisitions each. The ^{29}Si CP/MAS NMR spectra were collected at contact time of 10 ms using a ramped contact pulse on ^{1}H and contact r.f. frequencies of 100 and 83.4 kHz for ^{1}H and ^{29}Si, respectively, ^{1}H excitation (rf = 66.6 kHz), and ^{29}Si pulses (rf = 55.5 kHz) were calibrated using an external sample of kaolinite. The ^{29}Si{^{1}H} MultiCP NMR data were collected using the same r.f frequencies as the ramped CP using the composite pulse version of the Multi-CP experiment. For the Multi-CP experiment a total of 35 loops of a 2.42 ms contact pulse was used with a final contact time of 0.55 ms, a proton repolarization time of 0.2 s, and a 1.25 s acquisition delay. The durations of the contact times, delays, and number of cycles used for the Multi-CP experiment were optimized using the 50% MQ resin sample while all ^{29}Si spectra were referenced to kaolinite (δ_{Si} = -92 ppm).[34]

The ^{1}H SP/NMR and ^{1}H DQ NMR experiments were performed on a Bruker Avance III spectrometer operating at a proton Larmour frequency of 399.86 MHz using a Bruker HXY MAS probe with 4 mm (o.d.) zirconia rotors and polychlorotrifluoroethylene (PCTFE or Kel-F®) caps. An excitation pulse of 3.2 μs and a recycle delay of 10 s were used for both experiments. All experiments were conducted in the static state and samples were cut to fill the center coil volume of probe. DQ build up curves were measured using a pulse sequence (Figure S1) previously described in detail[28, 30, 32] which is designed to excite even-quantum coherences. ^{1}H DQ data was normalized according to previously established methods[22-25, 31] where relaxation effects are separated from network structural information with a point-by-point division of the DQ build up curve by a sum of the DQ intensity and the corrected reference intensity. Normalized build up curves were fit with Tikhonov regularization using a home-built Python program similar to the FTIKREG package.[32, 35] We employed the kernel function (eq 3) introduced by Chinn et al.[27] and described in detail by Chasé et al.[26] In this study, 55 DQ

excitation (τ_{DQ}) points were used to measure the DQ build-up curves with more points chosen at earlier excitation times to increase the reliability of the regularization results.

$$I_{nDQ}(\tau_{DQ}, D_{res}) = 0.5\left(1 - exp\left\{-\left(0.378 D_{res}\tau_{DQ}\right)^{1.5}\right\} \times \cos\left[0.583 D_{res}\tau_{DQ}\right]\right) \quad (3)$$

A hybrid fitting method was developed to derive estimated distributions of high RDC values (> 0.6 kHz/2π) that are poorly captured by the Tikhonov regularization method. The fitting technique used here is dependent on the distribution statistics obtained by fitting a series of gaussian curves to the low RDC portion (< 0.6 kHz/2π) of the distribution curve produced by Tikhonov regularization. The standard errors associated with the peak amplitudes, widths, and positions of the individual gaussian lines are used as boundary conditions for a Monte Carlo estimator which derives the distributions of high RDC values. The model progresses by adding a random error to each of the parameters of the gaussian lineshapes using the above boundary conditions and each line is summed to generate a new RDC distribution. A normalized DQ build-up curve is generated using eq 3 at each RDC value and weighted by the intensities of the newly generated distribution. This new DQ curve is used as a fixed fitting parameter in a minimization routine where the experimental data is fit by the new DQ curve and a second component representing a single instance of eq 3 is allowed to vary its intensity and RDC (Figure S2). The procedure is repeated 100,000 times to generate histograms of the high RDC distributions. The method also allows estimates of the standard deviation for the fractional abundance of the high RDC component as well as that for the mean value of the RDC. This model was implemented in a custom code written using the numpy and scipy packages of python 3.7. The full code is provided in the supporting information.

RESULTS AND DISCUSSION

Solvent Uptake and Mechanical Data. Simplified model network samples with varying amounts of MQ-resin were formulated by mixing a vinyl-terminated PDMS pre-polymer (32 kDa), a silane cross-linker (2-2.6 kDa), the vinyl-terminated MQ-resin, and a platinum catalyst. To approximate commercial silicone elastomer processing methods and to reduce sample formulation time, our model network samples were formulated as a two-part mixture that could easily be mixed in a 10:1 ratio to form the final networked samples. In this study, part A consisted of both the vinyl-terminated MQ-resin (up to 50 wt%) and the vinyl-terminated PDMS chains (32 kDA) while part B consisted of the cross-linker and a platinum catalyst. Lower concentration samples MQ-resin samples were made by diluting the MQ-resin containing part A with additional PDMS to achieve the desired MQ-resin concentrations (40, 30, 20, 10, and 2% MQ). However, the addition of part B to part A resulted in a slight dilution of the MQ-resin concentration of the final networked sample. As a result, the actual MQ content of each sample does not perfectly match the desired MQ content of each sample. The actual MQ content of each sample along with solvent uptake and mechanical data taken on the samples are displayed in Table 1 below. Solvent uptake experiments were used to determine network structure parameters such as the soluble fraction of material (% ω_{sol}) and the equilibrium degree of swelling (Q) as well as to compare the network structure of our materials to those previously studied.[15, 29] We also use the network properties determined from swelling and mechanical data as a standard metric for the network dynamics determined by NMR spectroscopy.

Sample	Actual Wt. % MQ	% ω_{sol}	σ	Equilibrium Degree of Swelling (Q)	σ	Young's Modulus	σ
0% MQ	0	4.8	1.6	3.5	0.05	0.57	0.14
2% MQ	2.1	NA	NA	NA	NA	NA	NA
10% MQ	9.1	4.3	1.7	3.4	0.03	1.13	0.02
20% MQ	18	3.3	0.9	2.5	0.01	1.92	0.05
30% MQ	27	4.0	0.9	2.0	0.03	3.31	0.08
40% MQ	36	3.4	1.6	1.8	0.01	6.67	0.51
50% MQ	45	3.5	1.2	1.8	0.06	17.9	0.47

Table 1. Actual MQ content present in each sample, results from solvent uptake, and results from mechanical analysis.

The soluble fraction of material determined from solvent uptake experiments remained relatively low across the samples, indicating that most of the starting materials were consumed, or cross-linked into the network during the cross-linking process. We observe a slight decrease in the soluble fraction of material as the MQ content increases, which could be an indicator of higher cross-linking efficiency as more MQ resin replaces the PDMS prepolymer. However, the standard deviation for these measurements is quite high. Given the large variability of the measurement itself, the change in soluble fraction of the materials is not statistically significant. When compared to previous studies, our 0% MQ sample has nearly double the soluble fraction (4.8% versus 2.8%) of a model network sample made with a 32 kDa PDMS pre-polymer that was demonstrated to have a very low defect fraction.[15] The difference in soluble fraction between the two model network samples is likely due to a change in the cross-linker in these new formulations. In the previously reported data, a small, tetrafunctional cross-linker was used to simplify the network chemistry as much as possible. Here, we employed a larger cross-linker (2 – 2.6 kDa) with multiple silane cross-linking sites (Scheme 1b). The networks studied here were also formulated with a much lower silane:vinyl ratio of 1.4 versus a 2-fold excess of silane in the

previously reported sample. The combination of a larger cross-linker and a lower excess of silane groups in the formulation chemistry could lead to less complete network formation and, therefore, a higher observed soluble fraction for these materials compared to similar model networks. Despite this observed increase in soluble fraction, we still expect that the network chemistry to be relatively complete for these samples. We used Raman spectroscopy to determine the degree of residual silane and vinyl groups within the networked samples reported here and those results will be discussed below.

The equilibrium degree of swelling (Q) is constant between the 0 and 10% MQ samples, then decreases with increased MQ content with the 40 and 50% MQ samples also having the same Q values of 1.8. While the decreased Q value with increasing MQ content reflects the higher cross-link density of the MQ-resins, the Q value only decreases by 1.7 when comparing the 0% and 50% MQ samples. The small change in Q value likely reflects a large degree of PDMS chain entanglements present in the base networked sample without MQ-resin. The Q value for the 0% MQ sample studied here is 3.5 compared to 3.9 and 4.8 for previously studied model networks with a similar size prepolymer.[15, 29] Although the comparative samples were formulated with the same molecular weight prepolymer they were both made with smaller sized cross-linker molecules. The use of a larger molecular weight cross-linker in this study combined with direct mixing of the network components without a diluting solvent resulted in a large degree of trapped chain entanglements that are reflected in the low Q value for the 0% MQ sample.[15] The high degree of trapped entanglements is further reflected in the small change in the Q value as the MQ content increases. Replacing the PDMS prepolymer with higher concentrations of MQ-resin leads to a smaller degree of equilibrium swelling both due to the trapped network entanglements that persist as the result of the higher molecular weight cross-

linker and the mixing conditions as well as the higher cross-link density of the MQ resins themselves. Overall, the solvent uptake data indicates that the model MQ networks studied here have a high degree of network entanglements that yield a high cross-link density before any MQ resin is added and that the cross-link density continues to increase with increasing MQ content to a maximum network cross-link density at 40% MQ.

The high degree of entanglements and increasing cross-link density in these model networks is further evidenced by the small changes observed in the Young's modulus from 0 to 30% MQ in Table 1. While the modulus doubles (0.57 to 1.13 MPa) from the 0 to the 10% MQ samples, there is only a slight increase in modulus when the MQ content is increased up to 30%. The initial increase in modulus when MQ-resin is added reflects the impact of cross-linking even small amounts of MQ-resin into the PDMS network. While the modulus increases between the 0 and 10% MQ samples, the degree of swelling does not change between these two samples. This result indicates that the replacement of 10wt% PDMS in this sample with MQ resin does not change the overall network cross-link density but does influence the network dynamics of the sample. This is likely due to the highly cross-linked nature of the MQ-resin molecules themselves which are designed to lend a reinforcing property to materials. At 40% MQ content the Young's modulus rises sharply to 6.7 MPa and rises sharply again to 17.9 MPa at 50% MQ. The sharp rise in Young's modulus above 30% MQ corresponds to a decline in the elongation at break value (Figure S3) as well as a low equilibrium degree of swelling value of 1.8. The dramatic increases in modulus above 30% MQ with the correspondingly low Q value and decreasing elongation at break are indicative of the dramatic increase in network cross-link density and resulting material hardness that occur when large amounts of MQ-resin are substituted for the more flexible PDMS chains. The swelling and mechanical data both reflect a

series of samples with two main structural and dynamic motifs. An entangled PDMS network with relative flexibility and cooperative molecular motions in addition to a more rigid domain dominated by the highly cross-linked MQ resin. At low and intermediate MQ content (up to 30% MQ) the more mobile PDMS network imparts enough elasticity to the offset the stiffness of the MQ resin. However, at MQ contents above 30% the mechanical properties of the MQ-resin begin to dominate the overall dynamics of the network resulting in an increase in the overall hardness and rigidity of the sample. The changes in network dynamics observed with solvent uptake and mechanical analysis are also supported by changes in the NMR data and will be discussed in more detail below.

Raman Spectroscopy. Figure 1a shows a Raman spectrum of the 50% MQ sample and Figure 1b shows the corresponding spectrum for the MQ resin alone. Both spectra are plotted on a logarithmic intensity scale. While many bands in the 50% MQ sample can be attributed to the MQ-resin, the band at ~ 616 cm^{-1} is strong and relatively well separated from bands attributed to PDMS. The band at 616 cm^{-1} has been assigned to the Si-C stretch of MQ-resins by Liang et al.[36] while the band near 490 cm^{-1} has been assigned to the Si-O-Si stretch of PDMS.[17-19] Comparison of the intensity of these two bands is the basis on which we have calculated the concentration of MQ-resin in each of the samples studied here. The spectral proximity of these two bands is an advantage because the effect of any instrumental sensitivity that is dependent on wavelength will be minimized. Finally, it is well known for PDMS[16, 17] and we have observed for MQ-resin that both bands are highly polarized. Hence, comparisons made using different instruments will likely be unaffected by different instrumental sensitivities to polarization state.

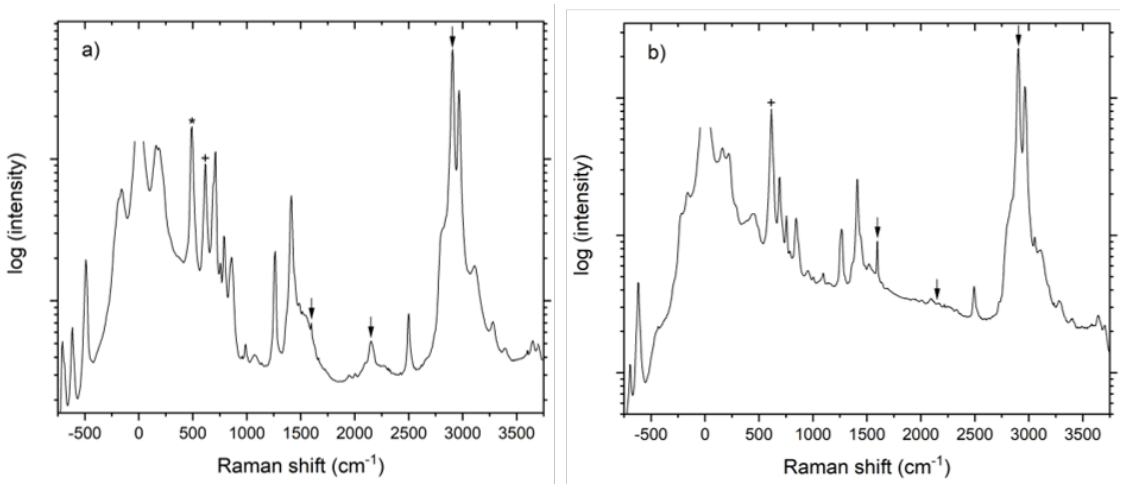

Figure 1. a) Raman spectrum of the cross-linked 50% MQ sample and b) Raman spectrum of the MQ resin alone. Intensities are plotted on a logarithmic scale. The asterisk and the cross indicate the PDMS and MQ bands, respectively, used to develop the calibration curve for MQ-resin concentration. Other relevant regions discussed in the text are indicated by the arrows.

A comparison of the relevant regions of the Raman spectra for the varying MQ content samples (Table 1) studied here is shown in Figure 2. The absolute contribution of the MQ band clearly increases with the addition of MQ-resin, while the intensity of the of PDMS band decreases as the MQ content increases. We created a calibration curve for determining the concentration of MQ-resin in silicone elastomers by taking the intensity ratio of the bands at 616 cm^{-1} (MQ-resin) and 490 cm^{-1} (PDMS). The intensity of each band was determined using two different methods: either by fitting the spectra with appropriate functions or by simple numerical integration of the areas under the bands. An example of the Lorentzian peak fitting results on the 50% MQ sample is shown in Figure S4. Higher resolution Raman spectra (Figure S5) reveal that the use of Lorentzian functions is an oversimplification of the peak shapes. However, Lorentzian lineshapes were demonstrated to give an adequate representation of the spectral lineshapes in lower resolution data, particularly at higher MQ concentrations. Lower resolution spectra can

also be obtained more rapidly, which is a practical advantage when determining MQ concentrations in unknown or commercial samples. We were able to detect the presence of MQ-resin in a sample containing 2.1% MQ (Figure S6), demonstrating that this detection method is effective at least down to that concentration. However, the MQ band is distorted by the overlap of native PDMS or impurity bands and a fit with a combination of simple functions was less successful (Figure S7).

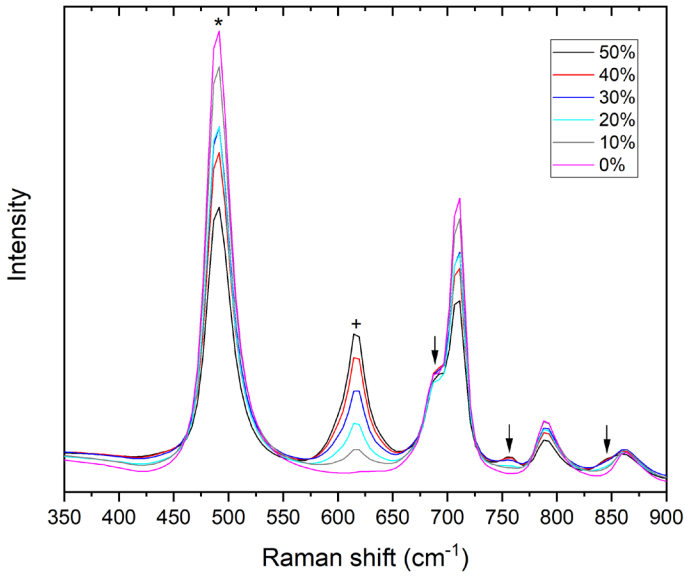

Figure 2. Comparison of Raman spectra of PDMS containing different weight percent MQ-resin. The bands labeled with an asterisk (PDMS) and a cross (MQ) are the bands that were used to develop the calibration curve. Other regions showing contributions from the MQ-resin are indicated with an arrow.

A plot of the peak intensity ratios of the PDMS and MQ-resin bands obtained by both peak fitting and numerical integration as a function of MQ content is shown in Figure 3. The observed upward curvature of the intensity ratios is the result of the PDMS concentration decreasing as more MQ-resin is added. The trend of the data is well described by a function of

the form $R = c - \frac{ax}{x-100}$ (red line), or equivalently $x = \frac{100(c-R)}{c-a-R}$. This implicitly assumes that there is no contribution of the MQ-resin in the spectral region of the PDMS Si-O-Si stretch, which is only an approximation. Fitting this function to the measured ratios (excluding the 2.1% wt. MQ sample) yields the red line with a = 0.616 ± 0.005 and c = 0.0003 ± 0.0029. Numerical integration (circles) was also used as an easier method to obtain the PDMS and MQ peak area ratios. While this approach is simpler than the peak fitting method, the integration limits are somewhat subjective. Nevertheless, the results obtained from numerical integration of the peaks are within the uncertainties derived from peak fitting. The calibration curve created here serves as a means for quickly and accurately determining the MQ content (down to 2% MQ) of cross-linked silicone elastomers. This method could be easily applied to commercial samples with unknown MQ content to determine not only if MQ resin is present, but also to quantify the amount of MQ present for an improved understanding of the structure-property relationships in silicones.

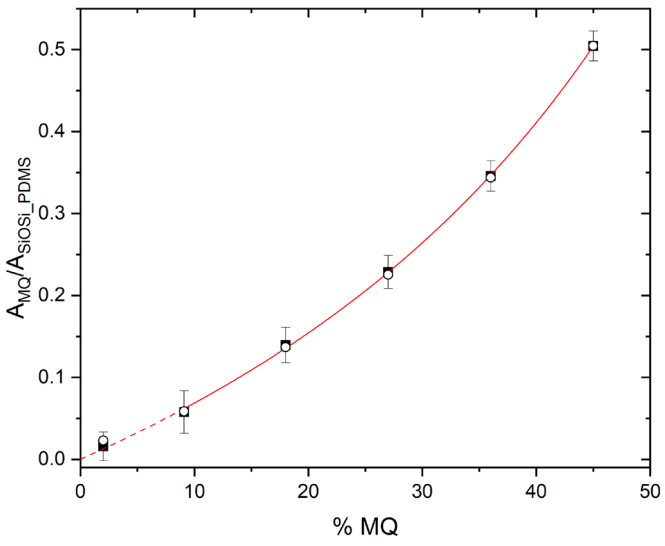

Figure 3. Intensity ratios of the MQ to the PDMS bands obtained from peak fitting (squares) and numerical integration (circles) as a function of MQ content. Error bars represent the propagated uncertainties due to peak fitting only. The red line is a fit to the peak ratios (excluding the 2% MQ sample). The dashed line is an extrapolation of the fit to 0% MQ.

In addition to developing a method for quantifying the concentration of MQ-resin using Raman spectroscopy, we have used the technique to evaluate the M/Q ratio of our samples. It was shown by Jayes et al.[37] that the Raman spectrum of MQ-resin could be used to infer the ratio of M to Q units. They did this by taking the ratio of the intensities of the symmetric C-H stretch band of the MQ-resin (~2905 cm^{-1}, also highly polarized) to the MQ band at ~616 cm^{-1} that we use in this study. In our case, the PDMS also contributes to the intensity in the C-H region. However, an estimate of the PDMS contribution to the C-H stretch can be obtained by first considering the ratio of the C-H band intensity (integration from 2833 cm^{-1} to 2942 cm^{-1}) to the Si-O-Si stretch in the PDMS sample without added MQ. Since the Si-O-Si band of PDMS is clearly resolved, even in MQ-containing materials, its intensity can be used to subtract the PDMS contribution to the C-H band. After subtracting the contribution of PDMS, we measured a ratio of 3.2 for the 50% MQ sample which corresponds to an M/Q ratio of 0.62 based on the study by Jayes et al.[37] Considering the assumptions and various sources of uncertainties in their measurements and ours (e.g. imperfect corrections for instrumental sensitivity across a wide spectral range), we conclude that for the samples studied here Raman spectroscopy is an effective tool for determining the type of MQ-resins contained in a PDMS network. This value is also in good agreement with the M/Q ratios (0.5 – 0.8) determined by NMR spectroscopy for the various batches of MQ resins synthesized in this study.

We also used Raman spectroscopy to investigate the completeness of the cross-linking reaction in our samples by identifying the presence of residual silane and vinyl groups (Figure 4). Although there are likely some artifacts in these weak spectral regions, we were able to assign some bands to these groups. The Si-H stretch of silane on the cross-linker was assigned to a band at a frequency of ~2150 cm^{-1} (Figure 4a) that is at a slightly lower frequency (~10 cm^{1}) than the silane frequency reported by Cai et al. and our measurement of the pure cross-linker (Figure S7).[18] The C=C stretch corresponding to vinyl groups on the PDMS chains and the MQ-resin were assigned to a band near 1600 cm^{-1} (Figure 4b).[18] The bands for both functional groups are generally weak compared with the uncured component materials (Figure S8), indicating that most of the silane and vinyl groups present in the samples are consumed during hydrosilylation. However, both bands increase in intensity at MQ concentrations of 30% and above indicating that the hydrosilylation reaction becomes less efficient as more MQ-resin is substituted for PDMS in the networked composite. While residual vinyl groups are present on both the PDMS chain ends and on the surface of the MQ resin particles, it is likely that unreacted PDMS chain ends would be subject to more steric hinderance than the small MQ-resin particles. As a result, we propose that the decrease in reaction efficiency with increased MQ content is largely the result of a small amount of unreacted PDMS chain ends. Despite the evidence of unreacted species via Raman spectroscopy, both the vinyl and silane peak intensities are low signifying that the hydrosilylation reaction is mostly complete in these samples.

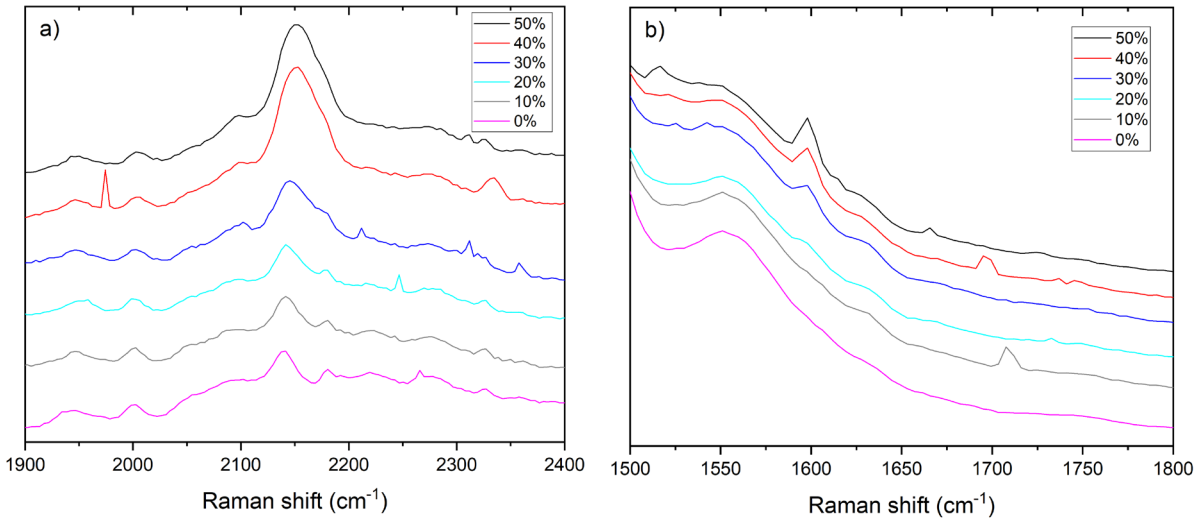

Figure 4. Raman spectra of networked samples containing various concentrations of MQ resin in the vicinity of a) the Si-H stretch and b) the vicinity of the C=C stretch. The spectra are vertically offset for clarity.

Static ^{1}H and ^{29}Si MAS NMR Spectroscopy. We applied a new MultiCP method[21, 38] not only to obtain ^{29}Si NMR data with an improved signal to noise ratio (S/N), but also to ascertain changes in the motional dynamics of the elastomers as a function of MQ content. In Figure 5 we observe that the ^{29}Si{^{1}H} MultiCP MAS NMR spectra produce the same peaks as we observe in ^{29}Si SP/MAS NMR experiments (Figure S9). However, the spectra collected using the MultiCP method have a better S/N ratio and required half of the acquisition time needed for the SP/MAS spectra. Although the MultiCP method was designed to be a quantitative experiment, the results for polymer systems with varying segmental dynamics are not quantitative due to the selective excitation of the less mobile species within the networked system. Despite the non-quantitative nature of the results, the MultiCP method has been demonstrated to have a more efficient nuclear spin polarization transfer in polymer networks with high mobility resulting in higher S/N and shorter acquisition times compared to SP NMR.[21] Furthermore, the dependence of the peak

intensity on the relative mobility of the structural motifs within the networked system in the MultiCP experiment can be used to extract information about the network dynamics when compared to peak intensities from static ^{1}H NMR and ^{29}Si SP/MAS experiments.

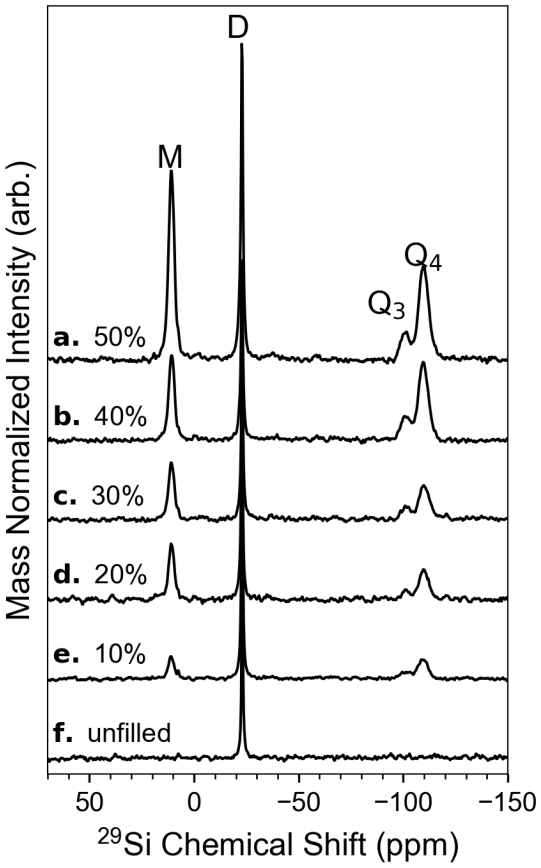

Figure 5. ^{29}Si Multi-CP MAS of model silicones with variable MQ contents.

Static ^{1}H NMR experiments (Figure S10) showed a single, broadened peak near 0 ppm which can be attributed to the methyl groups on the backbone of the PDMS polymer in addition to a broader signal that increased in intensity with the addition of MQ to the network. The broad, underlying peak is assigned to the methyl groups on the MQ species (Scheme 1). The relative concentration of MQ in each sample was determined by comparing the relative integrated area of these two peaks and are plotted as a function of MQ content in Figure 6a. These results show a

linear increase as a function of MQ content. Using this method, the MQ content of the 10, 20, 30, 40, and 50% samples were determined to be 10.4, 17.6, 25.6, 37.and 42.1% which are in good agreement (within a few percent) with the actual wt% MQ calculated from formulation data in Table 1.

The ^{29}Si SP/MAS (Figure S9) and the ^{29}Si MultiCP MAS spectra (Figure 5) contain four main peaks corresponding to M groups from the MQ-resin at 11.5ppm, D groups from the PDMS chain at -22.7 ppm, Q^3 groups from the MQ-resin at -100.8 ppm, and Q^4 groups from the MQ-resin at -109.1 ppm.[39] Integration of the D, Q, and M peaks in the ^{29}Si SP/MAS spectrum of the variable MQ samples was performed to provide a quantitative measurement of the MQ content of each sample similar to the static ^{1}H NMR data. The integrated ratio of (D+Q)/M groups suggest an MQ content of 6.3, 21.9, 27.7, 38.3, and 40.5% for 10 to 50% MQ samples. Given the lower S/N for the ^{29}Si SP/MAS spectra, these values compare well to that obtained from integration of the broad component of the static ^{1}H spectra, the MQ to PDMS ratio obtained from the Raman study, and the formulation data in Table 1 above. The relative agreement of these data sets combined with the linear trend in the ^{1}H NMR intensity suggests that the broad component from in the static ^{1}H spectra as well as the Raman peak ratios can be used as a direct, quantitative measure of the MQ content in silicone networks.

However, when the integrated peak areas of the M, D, and Q peaks in the ^{29}Si MultiCP MAS NMR data (Figure 6b) are used to calculate the concentration of MQ in each sample, the results are dramatically different from those calculated from the static ^{1}H NMR data. A plot of the difference of these measurements as a function of MQ content (Figure 6c) shows an observable trend that sheds light on relative spin dynamics of these samples. We observe that the relative difference between the static ^{1}H peak areas and the MultiCP peak areas decreases

linearly up to 50% MQ. We attribute this linear decline to a decrease in the fluctuations of the relative peak areas in the MultiCP data which results from the changing network mobility in the samples. The hypothetical MQ structure in Scheme 1 illustrates the rigid structure expected for the Q groups with increasing motional degrees of freedom expected for the M and D groups. Particularly if the M groups are not cross-linked into the PDMS network. In Figure 6b we show that the mass normalized areas for both the M and the Q peaks increase consistently as the MQ concentration increases. In contrast, the area for the D peak is relatively level across the MQ series until 50% MQ, where the area increases significantly. The constant behavior of the Q and M peaks suggests that during the MultiCP experiment these species are observing the same relative spin dynamics and that their areas are varying only due to their relative abundances in the sample series. However, we would expect the area of the D peak to decrease with increasing MQ content if the change in peak area were solely due to the change in formulation chemistry. Instead, the increased area of the D peak that we observe suggests that the dipolar couplings of the main PDMS chains are increasing with MQ content and, therefore, have a stronger contribution to the MultiCP results. These findings are further supported by the traditional ^{29}Si CP/MAS spectra collected (10 ms contact time) for the same samples (Figure S11) which show a dramatic increase in the total mass normalized signal intensity as the MQ the content increases. The increased signal intensity in both the MultiCP data and the traditional CP data is indicative of an overall decrease in the motion of the system as the MQ concentration increases. The observation of dramatically hindered network motion in the 50% MQ sample via the NMR data is also consistent with the modulus data (Table 1) which shows a dramatic increase in the hardness of the 50% MQ sample compared to the rest of the samples in the series. Furthermore, the dependence of the M peak areas on MQ concentration is consistent with MQ-resins that have

a high degree of cross-linking within the silicone network. If the MQ groups remained loosely cross-linked within the network, or if a large degree of M groups remained unreacted, then we would expect to observe a decreased dependence of the M park area with MQ content as is observed with the D peaks. The MultiCP data point toward a network model with highly cross-linked MQ resins that remain relatively immobile while the PDMS chain remains relatively mobile up to 50% MQ where the motion of the entire network is reduced enough to inhibit segmental motion of the PDMS chains in addition to the MQ resins.

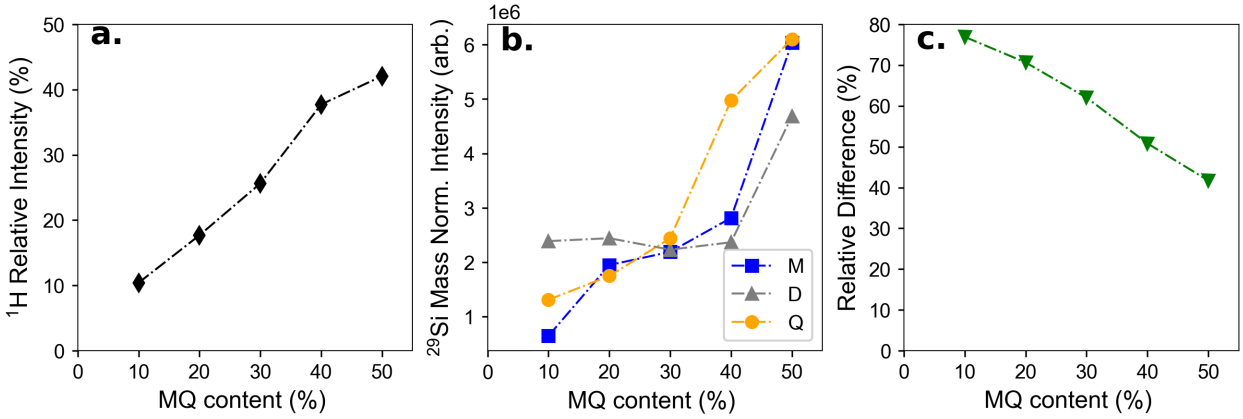

Figure 6. NMR derived integrated areas as function of the nominal MQ content. a) Relative ^{1}H area of the narrow and the broad underlying peak. b) Mass normalized areas derived from the ^{29}Si{^{1}H} MultiCP data. c) Relative difference in the MQ content derived from MultiCP and the ^{1}H data sets. Dashed lines are presented to guide the eye.

^{1}H DQ NMR Spectroscopy. The ^{1}H MQ NMR method allows for the quantification of dipolar coupling interactions between neighboring protons on polymer chains where topological constraints result in incomplete motional averaging of homonuclear (^{1}H-^{1}H) dipolar interactions. The residual dipolar couplings (RDC or D_{res}) are proportional to the dynamic chain order parameter, S_b, and the number of statistical segments between constraints, *N*.

$$S_b = \frac{D_{res}}{D_{stat}} = \frac{3}{5}\frac{r^2}{N}\langle P_2(\cos\alpha)\rangle \quad (4)$$

In the above expression, D_{stat} (8.9 kHz) is dipolar coupling in the absence of motion which is pre-averaged by the rotational methyl groups in PDMS, *r* is the vector describing the deviation of the end-to-end vector, **R**, from that of the unperturbed melt, $\mathbf{R}_o$ ($r = \mathbf{R}/\mathbf{R}_o$), and $P_2(\cos\alpha)$ is the second-order Legendre polynomial describing the time-averaged orientation changes between the dipolar vector and the chain axis. Multiple authors have demonstrated the relationship between residual dipolar couplings in elastomers well above the glass transition temperature to segmental dynamics of the polymer chains.[22-32]

^{1}H DQ growth curves along with RDC distribution curves produced from Tikhonov regularization are shown in Figure 7a-b. Although regularization resulted in well-defined RDC distributions at low RDC values ($\leq 0.6/2\pi$ kHz), the distribution curves are diffuse at higher RDC values and most do not descend towards zero intensity (Figure 7b). Investigation of the normalized DQ build-up curves (Figure 7a) reveals a significant residual intensity in the first data point for the 10-50% MQ samples and the intensity of that first data point consistently increases with increasing MQ content. The initial DQ excitation time (61.6 μs) shown here is the shortest excitation time obtainable using ^{1}H DQ NMR pulse sequence (Figure S1) developed by Saalwächter et al.[32] This pulse sequence selectively excites even numbered quantum coherences (2n + 2) and has been demonstrated to be stable a long DQ excitation times due to the addition of compensating π pulses that correct for pulse imperfections that can arise as the result of B_1 field heterogeneities in the elastomeric samples.[31, 32] While the stability at long DQ excitation times enables quantification of the DQ data, the extended length of a single excitation cycle excludes the measurement of strong residual dipolar coupling interactions (RDC > 10 kHz) and

complicates the quantification of moderate RDC interactions (3 – 10 kHz) as are present in the samples studied here.[31]

Further inspection of the ^{1}H DQ spectra produced during the first cycle of this pulse sequence reveals an underlying, broad contribution to the signal intensity (Figure S12) that is primarily responsible for the non-zero signal intensity at early tau times. We assign this broad contribution to the rapidly rotating methyl groups attached to the MQ-resin particles with restricted motional degrees of freedom due to their highly cross-linked network topology. The intensity of this feature increases with increasing MQ-resin content and the broad lineshape reflects high residual ^{1}H-^{1}H dipolar coupling values (short T_2 relaxation) that are in alignment with restricted molecular motion. The contribution of this broad peak to the non-zero signal intensity at short tau times results in the ill-defined high RDC distribution region (≥ 0.6 kHz/2π) produced by Tikhonov regularization of the DQ build-up curves (Figure 7b). The well-defined low RDC contribution (narrow peak in the ^{1}H DQ NMR spectra) to the RDC distribution curves is assigned to the more elastic and mobile PDMS network and is consistent with an average molecular weight between topological constraints close to the entanglement molecular weight of PDMS (as determined from equation 4).[27, 28, 40-43]

Analysis of the low RDC distribution curves (≤ 0.6 kHz/2π) produced from Tikhonov regularization (Figure 7c and Table 2) show a systematic shift of the mean position of the distribution to lower RDC values accompanied by slight a narrowing of the distribution curve that occurs from 0 to 30% MQ. Although the mean position of the RDC distributions for the 40 and 50% MQ samples does not change significantly from the 30% MQ sample, the full width at half maximum (FWHM) does increase with these samples. The small increase in FWHM for the

higher MQ content samples is the result of a small contribution at 0.4-0.6/2π kHz to the overall RDC distribution curve. The shift towards lower RDC with increasing MQ content indicates that the mobility of the PDMS network slightly increases with MQ content. This increase in mobility is likely the result of incomplete cross-linking of the vinyl terminated PDMS chain ends with increasing MQ content. While trapped entanglements and partial cross-linking of the PDMS chains would still restrict the overall motion of the PDMS network, the chain ends would represent a decreasing fraction of the overall vinyl content as the MQ concentration increases. In addition, steric hinderance would make cross-linking of networked PDMS chain ends less probable than cross-linking of the numerous vinyl groups (0.5 mmol/g) present on the small MQ-resin molecules. This observation is consistent with the Raman, swelling, and modulus data above. The Raman spectra show increased residual silane and vinyl content (Figure 4) with increasing MQ while the swelling and the modulus data (Table 1) indicate that the MQ resin is increasingly cross-linked into the network as the concentration increases. Particularly at the 40 and 50% concentrations. Therefore, we conclude that the residual silane and vinyl groups detected by Raman spectroscopy at 30% MQ and above are primarily the result of PDMS chains ends that are not cross-linked into the network. The decrease of PDMS cross-linking as MQ content increases leads to the more mobile PDMS phase that is reflected in the low RDC distribution curves. The small distribution present from 0.4/2π to 0.6/2π kHz could be the result of locally restricted chain motions due to trapped entanglements within the network. Although all the RDC distribution curves show some contribution in this region, only the 40 and 50% samples converge to zero intensity in this region and can be quantified.

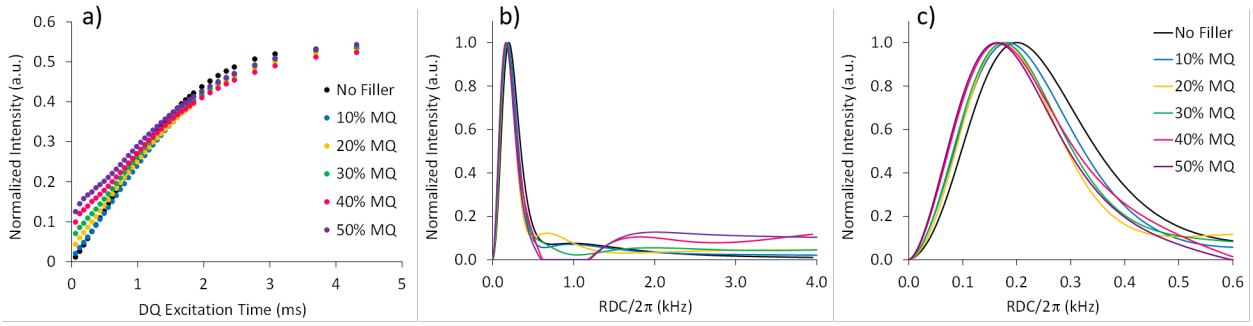

Figure 7. a) Normalized ^{1}H DQ build-up curves of variable MQ resins, b) residual dipolar coupling distribution results from Tikhonov regularization, and c) an expanded view of the low RDC region of the distribution curves.

Since Tikhonov regularization did not produce well-defined results at RDC values above 0.6/2π kHz, we attempted to simulate the high RDC distributions using the position and width data of the low RDC portion of the distribution curves as fitting constraints. The high RDC simulation results are shown in Table 2. The simulated distribution curves have mean positions and % contributions to the overall RDC distribution that increase regularly with the MQ content of the samples. Even the 0% MQ samples has a high RDC distribution at 0.86/2π kHz that is calculated to be 15% of the overall RDC distribution. The distribution centered at 0.86 could be the result of very small amounts of condensed cross-linking that would be structurally similar to an MQ-resin.[13-15] While we did not add any MQ resin to the 0% sample, the use of excess cross-linker combined with the implementation of an elevated-temperature post-curing step has been shown to result in the condensation of silane cross-linkers into structural motifs that are similar to MQ-resins. Given the amount of excess cross-linker used here (1.4 to 1) and the high cross-link density of the condensed cross-linker moiety, it would be a reasonable to assign the distribution at 0.86 RDC/2π to this MQ-like species. However, the overall contribution of 15% is

higher than the actual concentration of MQ-like species that would be present in the sample since Raman spectroscopy did not detect any MQ in this sample (< 2% MQ). Similarly, the simulated results yield a % contribution of the high RDC distribution in the 10 and 20% samples that is higher than the actual MQ content of the samples. At 30% MQ and above, the percent contribution of the high RDC curve to the overall RDC distribution is more in alignment with the actual MQ content of the samples. This not surprising since the % contribution of the high RDC component of the distribution curve reflects the contribution of the MQ species to the motional dynamics of the network for that sample and not necessarily the % MQ content in the sample. The simulated results indicate that even small amounts of MQ content or condensed cross-linker can modulate the motional dynamics of an otherwise very mobile sample network with a 15% contribution of more strongly coupled species present in the 0 and 10% MQ samples. Although this modulation is detectable in the DQ data, it still represents a minor contribution to the overall network dynamics that are still dominated by the elasticity of the PDMS network at low MQ concentrations. At 30% MQ and above the contribution of the high RDC component (less mobile network species) increases in alignment with the added MQ concentration which reflects the increased contribution of the MQ-resin itself to the overall hardening of PDMS-MQ composite networks. This is supported by the modulus data that shows a dramatic increase in material hardness at 40 and 50% MQ content. In addition to the increase in % contribution of the high RDC component, we also observe an increase in the mean position of the high RDC component as the MQ content increases which is also consistent with the modulus data. Both the experimental and the simulated ^{1}H DQ data are consistent with a series of MQ resin networks where the MQ significantly impacts the network dynamics at 40 and 50% MQ content, where the reinforcing effect of the MQ-resin is balanced by the elasticity and mobility of the entangled

PDMS network at moderate concentrations (20-30% MQ), and where the mobility of the PDMS network dominates the overall network dynamics at MQ concentrations of 10% and below.

Sample	Low RDC Average Postion (kHz/2π)	Low RDC Average FWHM	σ	Simulated Average High RDC (kHz/2π)	σ	Contribution of High RDC (%)	σ
0% MQ	0.24	0.20	0.08	0.86	0.12	15 (0)	1.8
10% MQ	0.22	0.20	0.08	1.05	0.29	15 (9.1)	2.8
20% MQ	0.20	0.16	0.07	1.31	0.15	25 (18)	3.0
30% MQ	0.21	0.19	0.08	1.50	0.25	29 (27)	3.6
40% MQ	0.22	0.22	0.09	2.64	0.17	36 (36)	1.1
50% MQ	0.21	0.21	0.09	3.66	0.32	42 (45)	1.5

Table 2. Low RDC results from Tikhonov regularization of the experimental build-up curves and simulation results for the high RDC region of the distribution curves. The actual MQ content of each sample from Table 1 is listed in parenthesis () under the contribution of high RDC column.

Although the experimental and simulated DQ data that we report here show trends that are consistent with the solvent uptake, mechanical, and high-resolution NMR spectroscopy we also recognize that a large part of our analysis of these data are based on simulations rather than direct regularization of the DQ data and may not be exactly representative of the actual network dynamics present in our samples. We continue to research multiple-quantum data collection and analysis methods that can be implemented to provide data points at lower excitation times (< 60 μs) in the DQ build-up curve and, therefore, improve regularization outcome. The development of more robust multiple-quantum NMR methods that can provide dynamic information on commercially relevant silicone formulations with complex chemistry and a large contribution of high RDC structural components will be explored in a follow-up publication. While detailed network structure information is readily available via ^{1}H DQ NMR on simplified PDMS systems,

the successful application of this technique to more complex commercial materials will provide much needed insights into the underlying network structure and dynamics that govern the materials properties of commercial silicones.

CONCLUSIONS

We have demonstrated that PDMS networks with MQ-resin used as a reinforcing filler are structurally and dynamically complex composites. These materials are cross-linked networks well above their glass transition temperature and such have no long-range order and are difficult to characterize using scattering techniques. The use of Raman and advanced NMR spectroscopies in this study has enabled improved insight into the structural features that influence the network and mechanical properties of this important class of composites. Raman spectroscopy is a sensitive detection tool for quantifying MQ-resin concentration down to at least 2% MQ, which makes it an important tool for the reverse engineering of commercial silicones. The ability of Raman spectroscopy to detect other structural moieties such as residual silane and vinyl groups at low concentrations also makes it a valuable tool for determining structure-property relationships in a variety of PDMS networks. In addition to demonstrating the utility of Raman spectroscopy as a quantitative diagnostic, we have also demonstrated that high-resolution solid-state NMR spectroscopy and ^{1}H DQ NMR spectroscopy are sensitive to changes in network dynamics as a function of MQ-resin content. Our application of the ^{29}Si MultiCP MAS NMR method enabled us to quantify the contributions of the MQ-resin and PDMS network to the overall network dynamics independently.

Lastly, experimental and simulated ^{1}H DQ results reflect the contributions of the networked PDMS chains, trapped entanglements, and the MQ-resin to the network dynamics that

are consistent with solvent uptake, mechanical analysis, and the MultiCP data. The combination of spectroscopic techniques applied here describe a series of samples where low MQ content (10%) has only a modest reinforcing effect on the PDMS network, where intermediate MQ contents (20-30%) yield networks with a more cooperative interplay between the reinforcing properties of the MQ resin and the mobility of the PDMS network, and where high MQ contents (40-50%) result in very rigid networks where the dynamics are dominated by the reinforcing properties of the MQ resins. The results presented here serve as the foundation for an improved understanding of the structure-property relationships in more complex commercial silicones which contain diverse cross-linking chemistries, heterogeneous filler phases, multimodal chain lengths, and the addition of various functional groups to the PDMS backbone. We anticipate that these Raman and NMR methods will be useful not only for the reverse engineering various commercial materials, but also for determining the mechanisms of aging and degradation of commercial silicones that are subject to environmental stressors including long-term compressive strain and thermal cycling during their service lifetimes.

ASSOCIATED CONTENT

Supporting Information

Figure S1. Schematic of the ^{1}H MQ pulse sequence used in this study.

Figure S2. Normalized build-up curves and fits produced from the hybrid fitting method used to simulate high RDC distributions.

Figure S3. Young's modulus (MPa) and elongation at break (%) plotted as a function of MQ-resin concentration in our model network samples.

Figure S4. An example of Lorentzian fits to the Raman spectrum of the 50% MQ sample.

LLNL-JRNL-817509

Figure S5. An example high-resolution Raman spectrum of the 50% MQ sample.

Figure S6. Expanded view Raman spectra of the 0% and 2% MQ samples.

Figure S7. Magnified view of the Raman spectrum for the 2% sample with fitting results.

Figure S8. Raman spectra of the starting materials used for our model network samples.

Figure S9. Comparison of the ^{29}Si SP/MAS, ^{29}Si MultiCP MAS, and ^{29}Si "traditional" CP/MAS data for the 50% MQ sample.

Figure S10. Example static ^{1}H NMR spectrum of the 50% MQ sample showing the broad and narrow contributions to the spectrum.

Figure S11. "Traditional" ^{29}Si CP/MAS results for the entire sample series.

Figure S12. An example of the ^{1}H DQ NMR spectrum for the first DQ excitation time (61.6 μs) of the 50% MQ sample.

AUTHOR INFORMATION

Corresponding Author

*E-Mail: (R.M.) maxwell7@llnl.gov

ACKNOWLEDGMENTS

We would like to thank N. Sobrepena for assistance with the Raman measurements. This work was performed under the auspices of the U.S. Department of Energy by Lawrence Livermore National Laboratory under Contract DE-AC52-07NA27344. This document was prepared as an account of work sponsored by an agency of the United States government. Neither the United States government nor Lawrence Livermore National Security, LLC, nor any of their employees

ABBREVIATIONS

Polydimethylsiloxane (PDMS)

Nuclear Magnetic Resonance (NMR)

Double Quantum (DQ)

Double-Quantum Nuclear Magnetic Resonance (DQ NMR)

Cross-Polarization Magic Angle Spinning (CP/MAS)

Cross-Polarization (CP)Single Pulse (SP)

Residual Dipolar Coupling (RDC)

REFERENCES

1. Mark, J. E., Some Interesting Things About Polysiloxanes. *Accounts of Chemical Research* **2004,** *37* (12), 946-953.

2. Warrick, E. L., *Forty Years of Firsts: The Recollections of a Dow Corning Pioneer*. 1 ed.; McGraw-Hill: 1990.

3. Paul, D. R.; Mark, J. E., Fillers for Polysiloxane ("Silicone") Elastomers. *Progress in Polymer Science* **2010,** *35* (7), 893-901.

4. Robeyns, C.; Picard, L.; Ganachaud, F., Synthesis, Characterization, and Modification of Silicone Resins: An "Augmented Review". *Progress in Organic Coatings* **2018,** *125*, 287-315.

5. Antosik, A. K.; Bednarczyk, P.; Czech, Z., Agin of Silicone Pressure-Sensitive Adhesives. *Polymer Bulletin* **2018,** *75*, 1141-1147.

6. Kuo, C.-F. J.; Chen, J.-B.; Shih, C.-Y.; Huang, C.-Y., Silicone Resin Synthesized by Tetraethoxysilane and Chlorotrimethylsilane Through Hydroslysis-Condensation Reaction. *Journal of Applied Polymer Science* **2013,** *131* (11).

7. Sun, F.; Hu, Y.; Du, H.-G., Synthesis and Characterization of MQ Silicone Resins. *Journal of Applied Polymer Science* **2012,** *125* (5), 3532-3536.

8. Lochhead, R. Y., *Cosmetic Science and Technology: Theoretical Principle and Applicaitons*. Elsevier: Cambridge, MA, 2017.

9. Lamoreaux, H. F.; Modic, F. J. Tough Unsupported Films Formed from Organopolysiloxanes. 3,629,358, 1971.

10. Modic, F. J. Silicone Potting Compositions Comprising Mixtures of Organopolysiloxanes Containing Vinyl Groups. 3,436,366, 1969.

11. Flagg, D. H.; McCarthy, T. J., Rediscovering Silicones: MQ Copolymers. *Macromolecules* **2016,** *49* (22), 8581-8592.

12. Tatarinova, E.; Vasilenko, N.; Muzafarov, A., Synthesis and Properties of MQ Copolymers: Current State of Knowledge. *Molecules* **2017,** *22* (10), 1768-1780.

13. Esteves, A. C. C.; Brokken-Zijp, J.; Laven, J.; Huinink, H. P.; Reuvers, N. J. W.; Van, M. P.; With, G. d., Influence of Cross-Linker Concentration on the Cross-Linking of PDMS and the Network Structures Formed. *Polymer* **2009,** *50*, 3955-3966.

14. Quan, X., Properties of Post-Cured Siloxane Networks. *Polymer Engineering and Science* **1989,** *29* (20), 1419-1425.

15. Sawvel, A. M.; Chinn, S. C.; Gee, M.; Loeb, C. K.; Maiti, A.; Mason, H. E.; Maxwell, R. S.; Lewicki, J. P., Nonideality in Silicone Network Formation via Solvent Swelling and ^{1}H Double-Quantum NMR. *Macromolecules* **2018,** *52* (2), 410-419.

16. Maxfield, J.; Shepherd, I. W., Investigation of Molecular Isomerism in Polydimethylsiloxane by Raman Scattering. *Chemical Physics* **1973,** *2* (4), 433-444.

17. Bae, S. C.; Lee, H.; Lin, Z.; Granick, S., Chemical Imaging in a Surface Forces Apparatus: Confolcal Raman Spectroscopy of Confined Poly(dimethylsiloxane). *Langmuir* **2005,** *21* (13), 5685-5688.

18. Cai, D.; Neyer, A.; Kuckuk, R.; Heise, H. M., Raman, Mid-Infrared, Near-Infrared an Ultraviolet-Visible Spectroscopy of PDMS Silicone Rubber for Characterization of Polymer Optical Waveguide Materials. *Journal of Molecular Structure* **2010,** *976* (1-3), 274-281.

19. Bistričić, L.; Borjanović, V.; Mikac, L.; Dananić, V., Vibrational Spectroscopic Study of Poly(dimethylsiloxane)-ZnO Nanocomposites. *Vibrational Spectroscopy* **2013,** *68*, 1-10.

20. Schmidt-Rohr, K.; Spiess, H., *Multidimensional Solid-State NMR and Polymers*. Academic Press Limited: San Diego, CA, 1994; p 496.

21. Duan, P.; Schmidt-Rohr, K., Composite-Pulse and Partially Dipolar Dephased MultiCP for Improved Quantitative Solid-State ^{13}C NMR. *Journal of Magnetic Resonance* **2017,** *285*, 68-78.

22. Chassé, W.; Lang, M.; Sommer, J.-U.; Saalwächter, K., Cross-Link Density Estimation of PDMS Networks with Precise Consideration of Network Defects. *Macromolecules* **2012,** *45* (2), 899-912.

23. Chassé, W.; Lang, M.; Sommer, J.-U.; Saalwächter, K., Correction to Cross-Link Density Estimation of PDMS Networks with Precise Consideration of Networks Defects. *Macromolecules* **2015,** *48* (4), 1267-1268.

24. Chassé, W.; Schlögl, S.; Riess, G.; Saalwächter, K., Inhomogeneities in Local Chain Stretching in Partially Swollen Networks. *Soft Matter* **2013,** *9*, 6943-6954.

25. Chassé, W.; Schlögl, S.; Riess, G.; Saalwächter, K., Correction: Inhomogeneities and local chain stretching in partially swollen networks *Soft Matter* **2015,** *11*, 4337-4338.

26. Chassé, W.; Valentín, J. L.; Genesky, G. D.; Cohen, C.; Saalwächter, K., Precise Dipolar Coupling Constant Distribution Analysis in Proton Multiple-Quantum NMR of Elastomers. *The Journal of Chemical Physics* **2011,** *134*, 044907-044910.

27. Chinn, S. C.; Alviso, C. T.; Berman, E. S. F.; Harvey, C. A.; Maxwell, R. S.; Wilson, T. S.; Cohenour, R.; Saalwächter, K.; Chassé, W., MQ NMR and SPME Analysis of Nonlinearity in the Degradation of a Filled Silicone Elastomer. *Journal of Physical Chemistry B* **2010,** *114* (30), 9729-9736.

28. Giuliani, J. R.; Gjersing, E. L.; Chinn, S. C.; Jones, T. V.; Wilson, T. S.; Alviso, C. T.; Herberg, J. L.; Pearson, M. A.; Maxwell, R. S., Thermal Degradation in a Trimodal Poly(dimethylsiloxane) Network Studied by ^{1}H Multiple Quantum NMR. *Journal of Physical Chemistry B* **2007,** *111* (45), 12977-12984.

29. Mayer, B. P.; Lewicki, J. P.; Weisgraber, T. H.; Small, W.; Chinn, S. C.; Maxwell, R. S., Linking Network Microstructure to Macroscopic Properties of Siloxane Elastomers Using

Combined Nuclear Magnetic Resonance and Mesoscale Computational Modeling. *Macromolecules* **2011,** *44* (20), 8106-8115.

30. Saalwächter, K., ^{1}H Multiple-Quantum Nuclear Magnetic Resonance Investigations of Molecular Order in Polymer Networks. II. Itensity Decay and Restricted Slow Dynamics. *The Journal of Chemical Physics* **2004,** *120*, 454-464.

31. Saalwächter, K., Proton Multiple-Quantum NMR for the Study of Chain Dynamics and Structural Constraints in Polymeric Soft Materials. *Progress in Nuclear Magnetic Resonance Spectroscopy* **2007,** *51*, 1-35.

32. Saalwächter, K.; Ziegler, P.; Spyckerelle, O.; Haidar, B.; Vidal, A.; Sommer, J.-U., ^{1}H Multiple-Quantum Nuclear Magnetic Resonance Investigations of Molecular Order Distributions in Poly(dimethylsiloxane) Networks: Evidence for a Linear Mixing Law In Bimodal Systems. *The Journal of Chemical Physics* **2003,** *119*, 3468-3482.

33. Xu, X.; Wu, C.; Zhang, B.; Dong, H., Preparation, Structure Characterization, and Thermal Performance of Phenyl-Modified MQ Silicone Resins. *Journal of Applied Polymer Science* **2013,** *128* (6), 4189-4200.

34. Magi, M.; Lippmaa, E.; Samoson, A.; Engelhardt, G.; Grimmer, A. R., Solid-State High-Resolution Silicon-29 Chemical Shifts in Silicates. *The Journal of Physical Chemistry* **1984,** *88* (8), 1518-1522.

35. Weese, J., A Reliable and Fast Method for the Solutio of Fredholm Integral Equations of the First Kind Based on Tikhonov Regularization. *Computer Physics Communications* **1992,** *69* (1), 99-111.

36. Liang, W.; Ge, X.; Ge, J.; Li, T.; Zhao, T.; Chen, X.; Song, Y.; Cui, Y.; Khan, M.; Ji, J.; Pang, X.; Liu, R., Resin Non-Aggregates for Silicone Rubber Composites with Enhanced Thermal Conductivity and Mechanical Performance. *Polymers* **2018,** *10*, 1254-1255.

37. Jayes, L.; Hard, A. P.; Séné, C.; Parker, S. F.; Jayasooriya, U. A., Vibrational Spectroscopic Analysis of Silicones: A Fourier Transform-Raman and Inelastic Neutron Scattering Investigation. *Analytical Chemistry* **2003,** *75* (4), 742-746.

38. Johnson, R. L.; Schmidt-Rohr, K., Quantitative Solid-State 13C NMR with Signal Enhancement by Mulitple Cross Polarization. *Journal of Magnetic Resonance* **2014,** *239*, 44-49.

39. Beshah, K.; Mark, J. E.; Ackerman, J. L.; Himstedt, A., Characterization of PDMS Model Junctions and Networks by Solution and Solid-State Silicon-29 NMR Spectroscopy. *Journal of Polymer Science Part B: Polymer Physics* **1986,** *26* (6), 1207-1225.

40. Chinn, S.; DeTeresa, S.; Sawvel, A.; Shields, A.; Balazas, B.; Maxwell, R. S., Chemical Origins of Permanent Set in a Peroxide Cured Filled Silicone Elastomer - Tensile and ^{1}H NMR Analysis. *Polymer Degradation and Stability* **2006,** *91* (3), 555-564.

41. Gjersing, E.; Chinn, S.; Giuliani, J. R.; Herberg, J.; Maxwell, R. S.; Eastwood, E.; Bowen, D.; Stephens, T., Investigation of Network Heterogeneities in Filled, Trimodal, Highly Functional PDMS Networks by H-1 Multiple Quantum NMR. *Macromolecules* **2007,** *40* (14), 4953-4962.

42. Maxwell, R. S.; Chinn, S. C.; Alviso, C. T.; Harvey, C. A.; Giuliani, J. R.; Wilson, T. S.; Cohenour, R., Quantification of Radiation Induced Crosslinking in a Commercial, Toughened Silicone Rubber, TR55 by H-1 MQ-NMR. *Polymer Degradation and Stability* **2009,** *94* (3), 456-464.

43. Mayer, B. P.; Chinn, S. C.; Maxwell, R. S.; Reimer, J. A., Solid State NMR Investigation of Gamma-Irradiated Composite Siloxanes: Probing the Silica/Polysiloxane Interface. *Polymer Degradation and Stability* **2013,** *98* (7), 1362-1368.

Spectroscopic Signatures of MQ-Resins in Silicone Elastomers

April M. Sawvel[1], Jonathan C. Crowhurst[1], Harris E. Mason[2], James S. Oakdale[1], Samantha Ruelas[1], Hannah V. Eshelman[1], and Robert S. Maxwell[,1].*

[1]Physical and Life Sciences Directorate, Materials Science Division, Lawrence Livermore National Laboratory, 7000 East Avenue, Livermore, CA 94550.

[2]Physical and Life Sciences Directorate, Atmospheric, Earth, and Energy Division, Lawrence Livermore National Laboratory, 7000 East Avenue, Livermore, CA 94550.

SUPPORTING INFORMATION

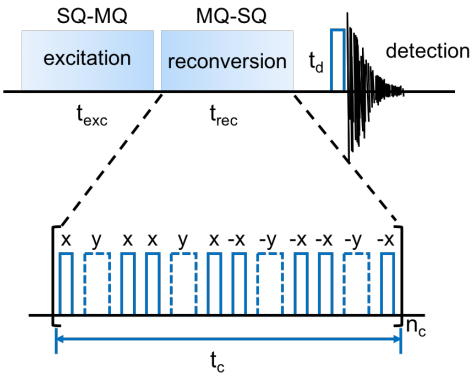

Figure S1. ^{1}H MQ pulse sequence used in this study. Solid lines represent π/2 pulses and dashed lines represent π pulses. The number of pulse trains (n_c) was incremented to generate growth

curves. Reference MQ coherences, containing all excited 4*n* quantum orders, were selected using the DQ (double quantum) selection phase cycle without receiver alternation.

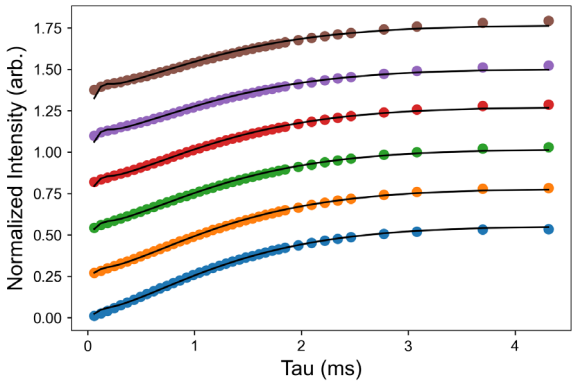

Figure S2. Normalized DQ build-up curves and fits produced using our hybrid fitting method. The curves start with the 0% MQ sample at the bottom (blue) and then go through the series of samples from 10 to 50% MQ. The curves have been offset in this Figure for clarity.

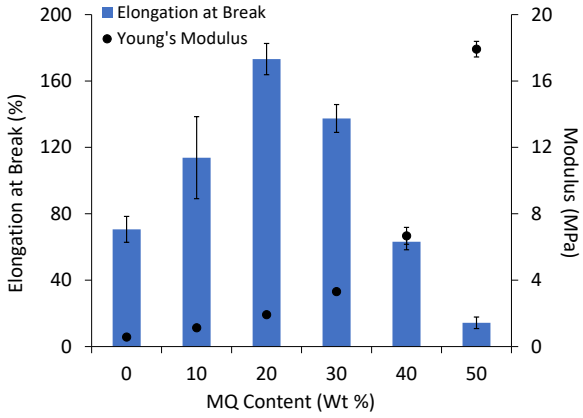

Figure S3. Young's modulus (MPa) and elongation at break (%) plotted as a function of MQ-resin concentration in our model network samples. A sharp decline in the elongation at break

value above 30% MQ-resin content corresponds with the observed sharp increase in the Young's modulus value of these samples.

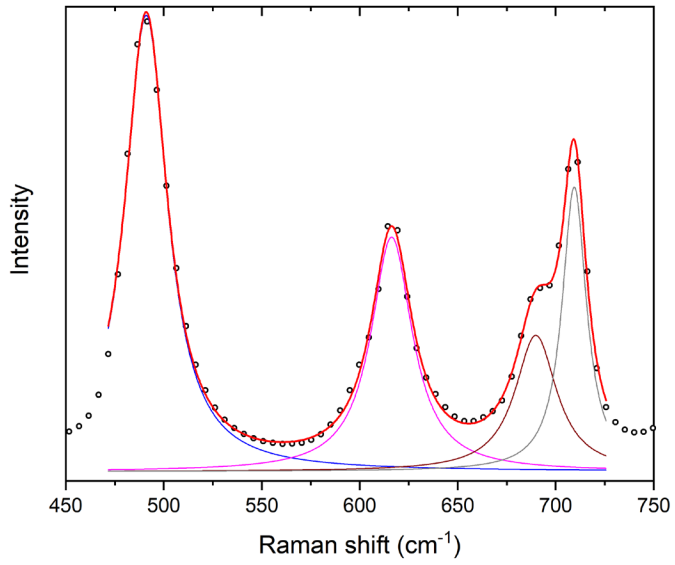

Figure S4. The region of the Raman spectrum of the 50% MQ sample relevant to the calibration curve shown in the main text. A sum of Lorentzian functions was fitted to the spectrum after a linear background subtraction. The various components are indicated as well as their cumulative line shape.

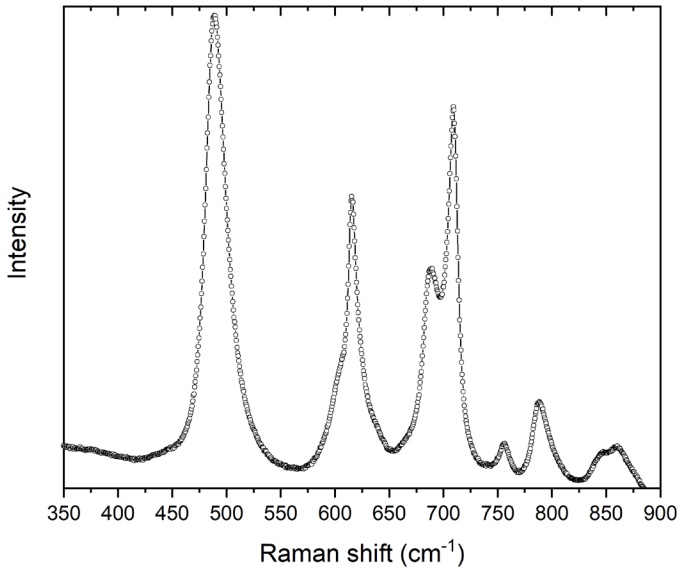

Figure S5. High resolution Raman spectrum of the 50% MQ sample. The spectral region covers the same range as that of Figure 2 of the main text.

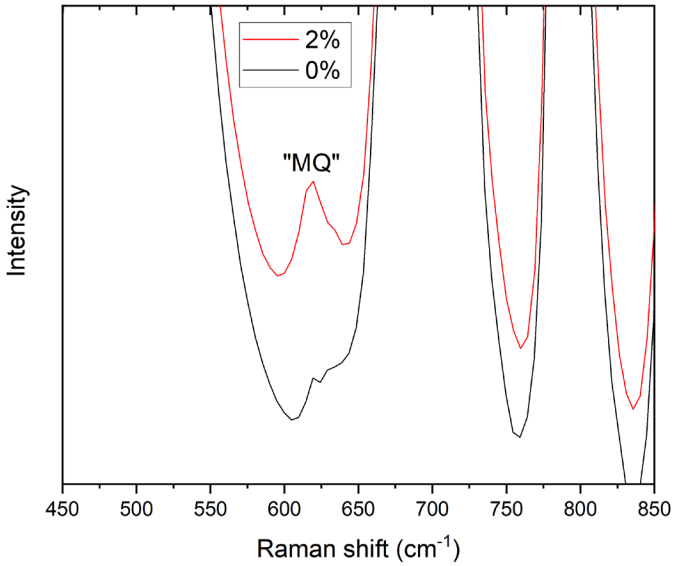

Figure S6. Raman spectra of the 0% MQ sample compared to the 2% MQ sample. Spectra normalized to the Si-O-Si stretch of PDMS. There is activity in the MQ region even in the 0% MQ sample, possibly due to MQ-like moieties created from condensed cross-linker.

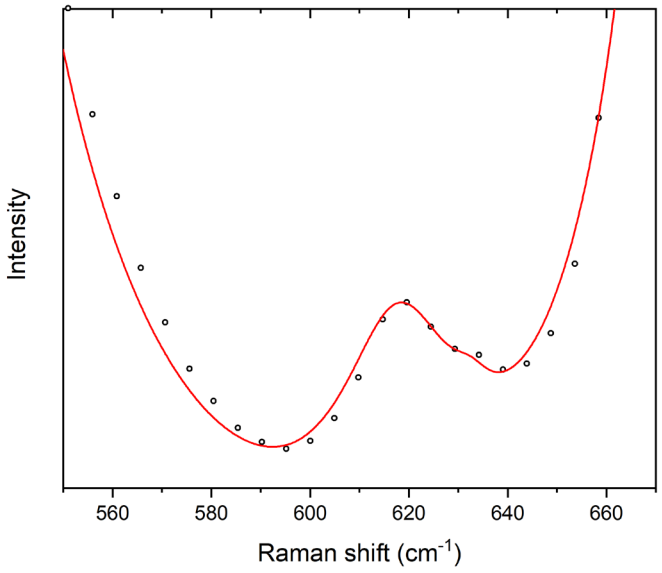

Figure S7. Magnified Raman spectrum of the 2% MQ sample. Solid line is a fit to the spectrum. Five Lorentzian components were used (instead of 4 as in Figure S2) to capture the weak contribution from the native material in the MQ spectral region.

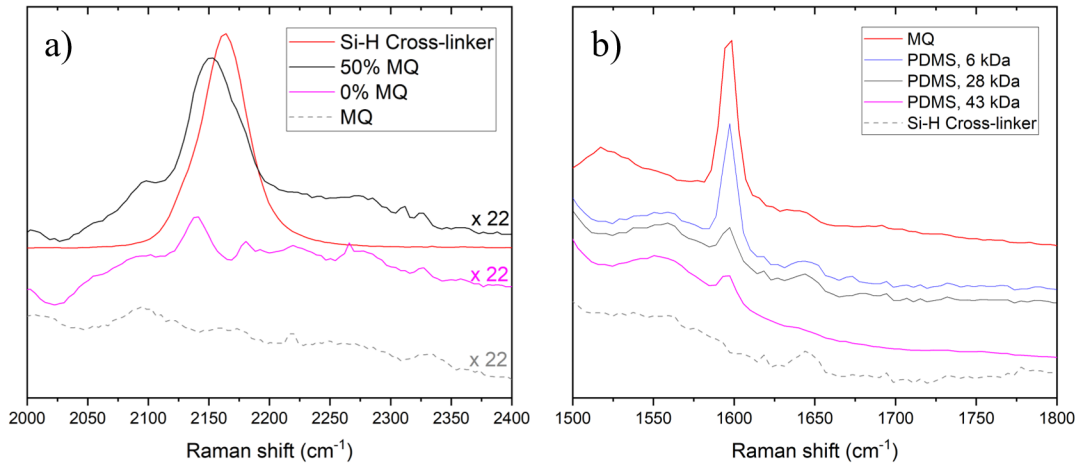

Figure S8. Raman spectra of the a) Si-H stretch region for the cross-linker (HMS-H271), the 50% MQ sample, the 0% MQ sample, and pure MQ-resin. b) Raman spectra of the C=C stretch region for pure MQ-resin, the cross-linker (HMS-H271), and three different molecular weight

PDMS chains (DMS-V21 = 6 kDa, DMS-V31 = 28 kDa, and DMS-V33 = 48 kDa). Raman spectra have been scaled and shifted vertically to permit comparison.

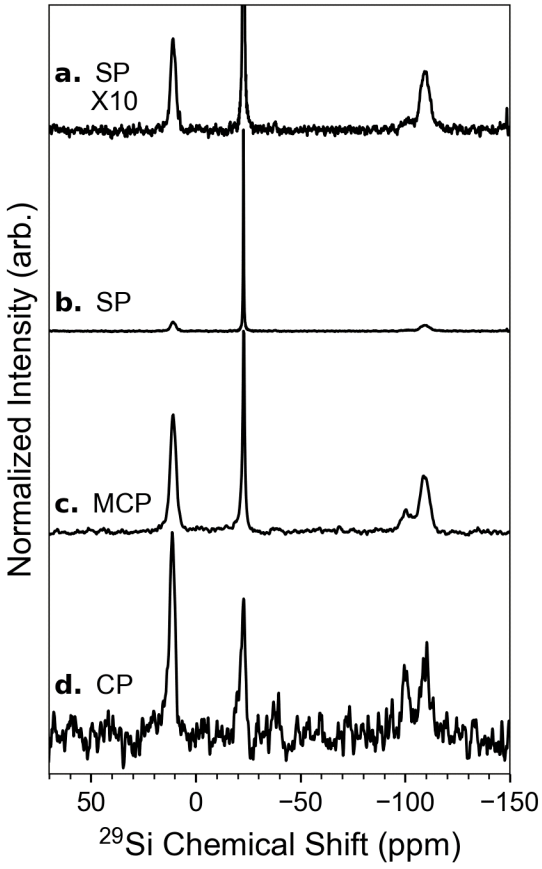

Figure S9. Comparison of a-b) ^{29}Si SP/MAS, c)^{29}Si{^{1}H} MultiCP, and d) traditional ^{29}Si{^{1}H} CP/MAS experiments collected on the 50% MQ Resin sample.

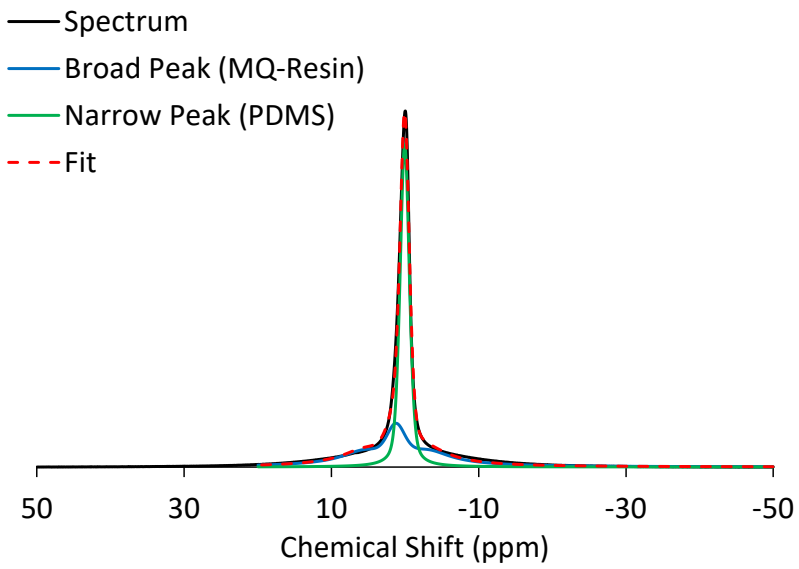

Figure S10. Static ^{1}H NMR spectra of the 50% MQ sample showing the broad spectral component that increases in intensity with MQ content.

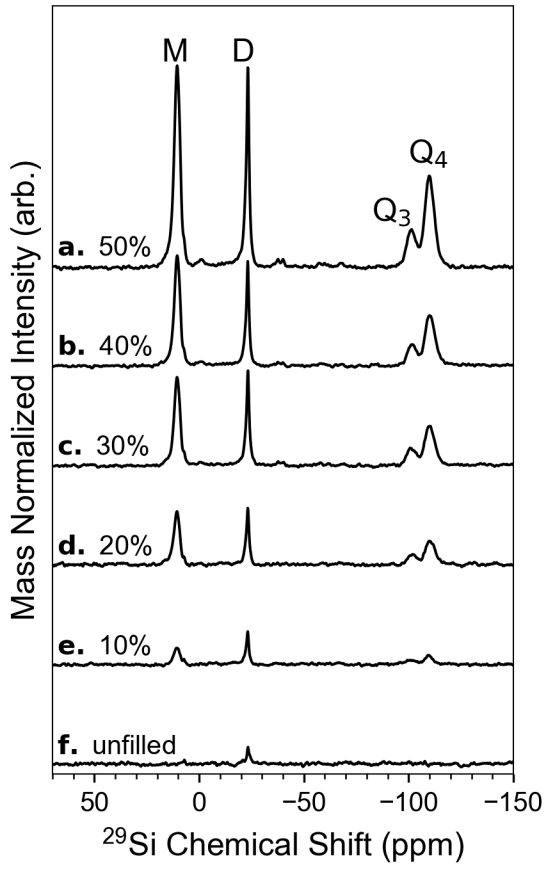

Figure S11. "Traditional" $^{29}Si\{^{1}H\}$ CP/MAS spectra collected using a 10 ms contact pulse for the MQ samples in descending order of MQ content. The intensities have been scaled relative to the number of scans and normalized to the sample mass.

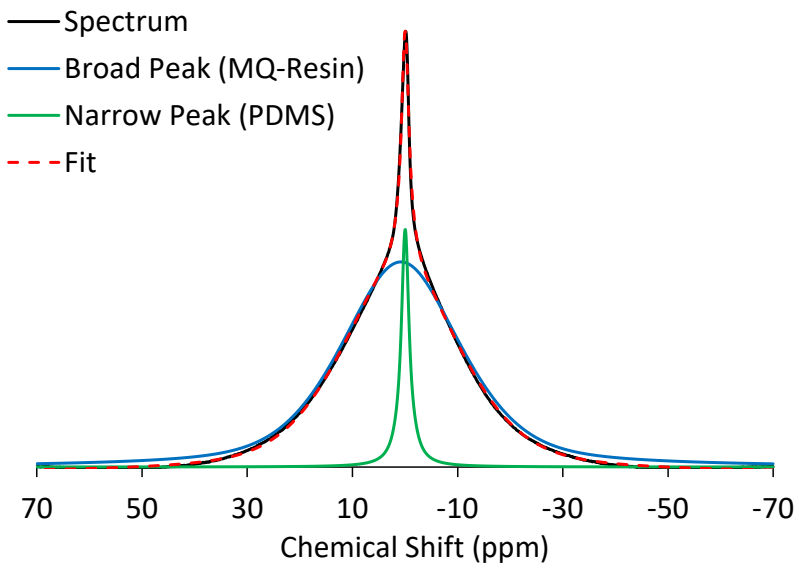

Figure S12. An example of the ^{1}H DQ NMR spectrum for the first DQ excitation time (61.6 μs) of the 50% MQ sample. The broad underlying component increases in intensity with MQ content and has been assigned to the high ^{1}H-^{1}H dipolar coupling interactions in the MQ-resin.